

Bearing and Cleavage Failure Simulation of Single Lap Bolted Joint Using Finite Element Method

Mohammad Ali Saeimi Sadigh¹ · Gholamreza Marami²

Received: 31 August 2015 / Accepted: 23 October 2015 / Published online: 1 February 2016
© The Indian Institute of Metals - IIM 2016

Abstract This paper deals with the distortion and failure behavior of the single lap bolted joints with similar and dissimilar substrates experimentally and numerically. Nonlinear finite element (FE) model has been used to simulate excessive distortions and failure modes of the assemblies. FE results show that elasto-plastic model has sufficient accuracy in predicting the distortion behavior of the models with only bearing failure. However, this model has less accuracy compared to other models with Mixed-Mode (Bearing + Cleavage) failure. Therefore, in this paper, an energy based failure criteria has been used to simulate the joint distortions and rupture. Results show that the joint behavior can be accurately simulated using the above mentioned failure criterion.

Keywords Single lap bolted joint · Finite element · Damage simulation

1 Introduction

Removable joints such as bolted assemblies are frequently employed in aeronautics, automotive and railway industries. These joints are frequently employed in assembling various components. However, the presence of geometric

discontinuities due to hole-drilling constitutes weak point in the bolted joints, since this leads to stress concentration in the bolted joints [1]. Stress concentration is one of the main reasons of failure in the bolt connected assemblies. Therefore, several researches have been focused on the failure mechanisms of the bolted joints under tension-shearing [2]. Designing bolted assemblies, requires control of static [3], dynamic [4] and fatigue [5] behaviors. Because of this, experimental methods [6], analytical models [7] and finite element (FE) analysis [8] are implemented to investigate the mechanical characteristics of the bolted assemblies. These investigations include several aspects like stress concentration [1], influence of clearance between the hole [9], tightening torque effects and bolt shank and different modes of joint failure [10].

One or mixed failure modes effect the ultimate strength of a bolted connection. These failure modes include bearing, end pull-out, net section fracture, bolt shear, block shear rupture, etc. Chung et al. [3] established a FE model to study the structural behavior of bolted joint. They have shown that, on using the FE model, bearing, shear-out and net section failure modes can be predicted successfully. Hoang et al. [6] studied the influence of tightening torque and clearance on the failure characteristics of the bolted assemblies. They have also used image processing method to analyze sequence of damage mechanisms. Additionally, they have studied the failure modes of the bolted lap joints experimentally and numerically [8, 10]. They have reported that, two geometrical parameters play the most important role in the failure modes of a bolted joint under tension. First is the percentage of net section of the plate which resists the tensile load and second is the percentage of the useful area of plate that resists shear load. Salih et al. [11] investigated the net section failure behavior of austenitic and ferritic stainless steel joints. They have developed

✉ Gholamreza Marami
gh.marami@srbiau.ac.ir

Mohammad Ali Saeimi Sadigh
saeimi.sadigh@azaruniv.ac.ir

¹ Department of Mechanical Engineering, Azarbaijan Shahid Madani University, Tabriz, Iran

² Department of Mechanical Engineering, Tabriz University, Tabriz, Iran

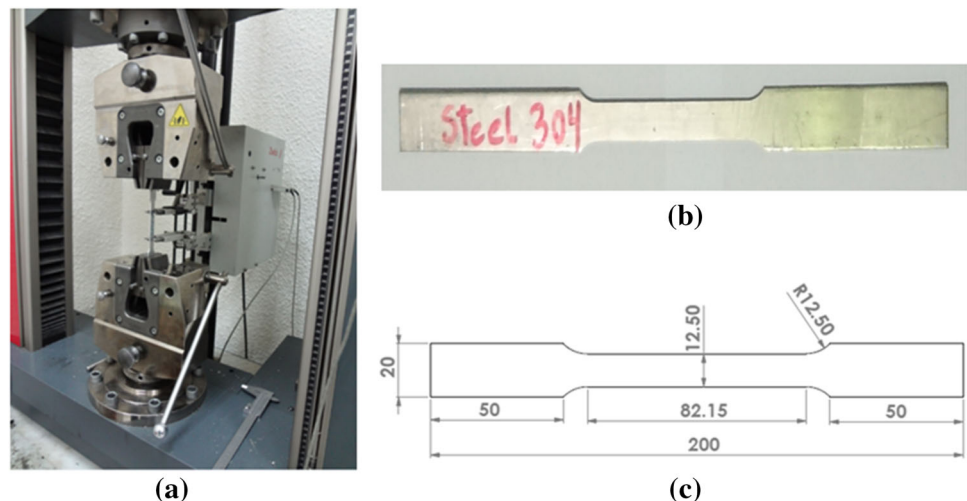
numerical models for these joints and have proposed a modified design equation using the numerical and experimental results. Yun et al. [12] performed a study to improve the strength of the multi-bolted connections. They experimentally demonstrated that, load acts uniformly in these joints with positive hole clearance comparing to the joints without clearance. Therefore the multi-bolted joints with positive clearance exhibit 13.1–21.8 % failure strength improvement.

The aim of the current research is to simulate the distortion and failure behavior of the single lap bolted joints with similar and dissimilar substrates. Three case studies are defined using thin sheets of aluminum alloy 7075-t6 and stainless steel 304. Uni-axial tensile tests are conducted and the joints distortions during the tests are measured. Then three dimensional FE based model is employed to simulate the global distortion behavior and failure of the joints.

2 Experimental Procedures

In this research, failure of the bolted single lap joints made from similar and dissimilar substrates were investigated. The materials of the Substrates were steel 304 and aluminum 7075-T6, which were extracted from sheets with $t = 2$ mm thickness. The rolled sheets exhibited different characteristics in longitudinal and transverse directions. In this analysis, all the specimens were prepared along longitudinal direction. Mechanical properties of the plates were obtained from the uni-axial tensile test. In order to carry out this test, standard specimens were prepared according to ASTM: E8M. Uni-axial tensile tests were conducted using Zwick tensile test machine with 50 kN capacity and 0.01 N accuracy load cell (see Fig. 1). The specimens were tested at 1 mm/min cross-head displacement rate. Contact extensometers with accuracy of $\pm 1 \mu\text{m}$ were used to record the specimen elongation.

Fig. 1 Tensile test. **a** Zwick tensile test machine, **b** test specimen, **c** test specimen dimensions



Since these materials demonstrated large inelastic strains, large deformations were expected to occur in the assembly. Therefore, true stress and true strain curves were needed for the numerical simulations. With this aim, nominal stresses (σ_{nom}) and nominal strains (ϵ_{nom}) were transformed into the corresponding true stresses and true strains using the following relationships:

$$\sigma_{true} = \sigma_{nom}(1 + \epsilon_{nom}) \quad (1)$$

$$\epsilon_{true} = \ln(1 + \epsilon_{nom}) \quad (2)$$

Figure 2 presents the true stress–strain curves of the aluminum alloy and stainless steel which were calculated using Eqs. (1) and (2). As can be seen from these figures, true stress continuously rises ahead of the nominal ultimate stress until the fracture occurs.

Two types of specimens with similar and dissimilar substrates were tested in single lap joints. Table 1 shows the three different case studies. Case studies 1 and 2 consisted of the assemblies with similar substrates and case study 3 involved the assemblies with dissimilar substrates.

Figure 3 illustrates the dimensions of the single lap bolted assembly. Fasteners are hex head M10 (grade 10.9) stainless steel bolts with tensile strength of 1040 MPa, yield stress of 940 MPa and proof strength of 830 MPa. High strength bolt was selected to study the failure in the substrates. A washer was used under the nut to achieve uniform compressive load distribution in the substrates. The clearance between the bolt shank and hole was 0.5 mm. The joints were assembled by applying an appropriate tightening torque. This torque creates preload at the bolt shank. In this project, the pretension load was fixed at 36 kN corresponding to the 75 % of bolt proof load. However, the preload value uncertainty arises during the clamping of the assembly because of different friction coefficient values between the bolt and

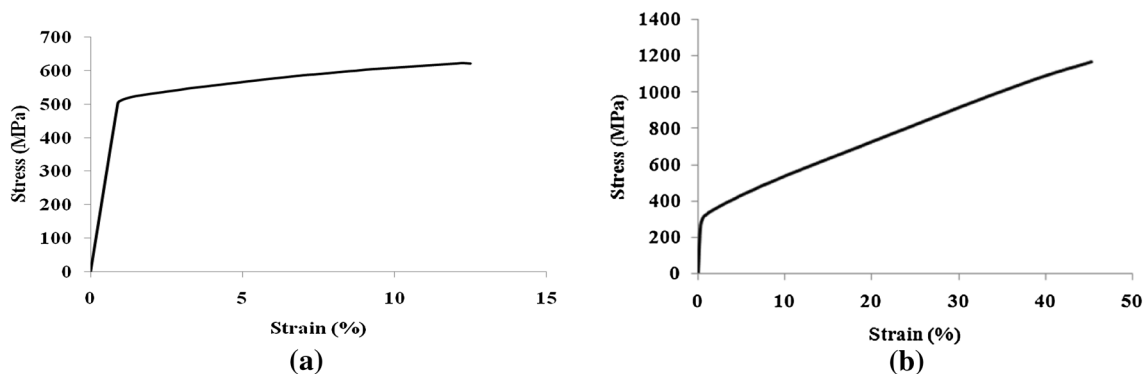


Fig. 2 True stress–strain behavior of **a** aluminum alloy, **b** stainless steel

Table 1 Different case studies

Case studies	Plate A	Plate B
1	Steel 304	Steel 304
2	Al 7075-T6	Al 7075-T6
3	Steel 304	Al 7075-T6

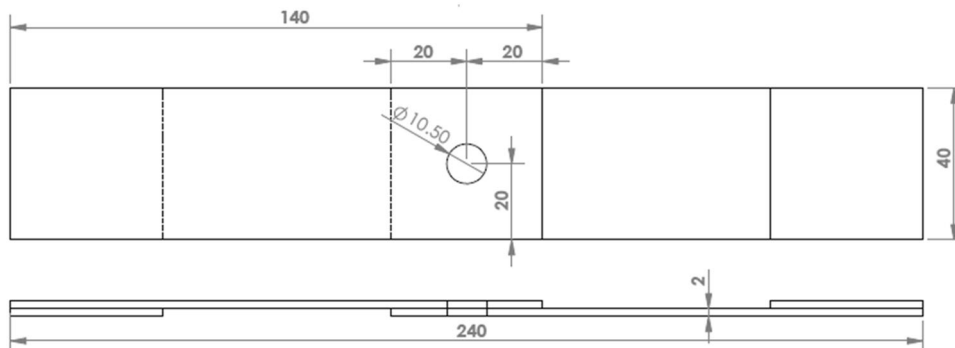
nut threads and washer. Therefore, the tightening torque which creates relevant preload was obtained experimentally. For this purpose, the method described in the Ref. [8] was used to obtain the corresponding torque. From this procedure, the magnitude of the torque which generated 36 kN load at the bolt shank was found to be 74 N m. Also, clamping force magnitude could be estimated using Eq. 3 [13]. In this equation, T is tightening Torque, d is the bolt nominal diameter and K is the torque coefficient. The average value of K for non lubricated surface with 0.15 friction coefficient value; is 0.2 [13]. Based on this equation, 37 kN clamping force is generated in the bolt shank if 74 N.m torque is applied to the assembly which is close to the value obtained from the practical method. Finally, the joints were assembled with 36 kN pretension load.

$$F_c = \frac{T}{Kd_{bolt}} \tag{3}$$

3 Finite Element (FE) Modeling

In this research, FE package ABAQUS has been used to simulate the structural behavior of bolted joints. Three dimensional solid elements with incompatible mode (C3D8I) has been used to simulate the components of bolted assembly. In this element, bending behavior is improved by adding incompatible deformation modes in addition to the displacement degrees of freedom. In usual displacement elements, parasitic shear stresses occurs when they are loaded in bending. Parasitic shear stresses can be eliminated by adding the degrees of freedom. Also, Poisson’s effect, which results in artificial stiffening in the elements is eliminated in bending. In addition, the incompatible modes can avoid the inaccurate stresses and stiffness overestimation which are observed in common displacement elements. It is worth noting that the linear variations of the axial stresses together with the linear variations of the stresses perpendicular to the bending direction causes stiffness overestimation in common elements.

Fig. 3 Dimensions in mm of the lap joint



In current research, a nonlinear problem has been solved using FE method. In a bolted joint three common sources of nonlinearities, i.e. material, geometry and boundary condition are included in the FE models using elasto-plastic material model, NLGEOM command and contact element definition respectively. The loads are applied in small increments and equilibrium equations are solved using Newton–Raphson method. Then the residuals are checked to be within the defined tolerance, otherwise the increments are ignored and the procedure is repeated with smaller increments. Convergence of nonlinear problems is enormously difficult and program terminates in several cases because of numerical instability. In the current study, small elements have been used at the contact region, and the minimum value of the increment has been set to $1e-9$. In addition, line search method has been used to help the convergence.

Surface to surface contact elements are defined between all contacting surfaces of the plates and bolt. These elements are used to transfer load between surfaces that interact with each other. In contact modeling between the bodies, one surface is defined as master (deformable body) and the other is taken as slave (rigid body). In this study, for similar joints, master and slave surfaces are selected arbitrarily. However, for dissimilar joints, slave surface is assigned for bodies with higher rigidity. The software recognizes surfaces that are in contact using the master–slave algorithm and employs constraints to prevent penetration of the master and slave nodes. Friction coefficient of 0.15, 0.35 and 0.45 between the steel–steel, aluminum–aluminum and steel–aluminum materials have been used respectively. These values between the contacting pairs are obtained using a simple test. In this test a small piece of the material slides on the sloped surface of the same material under its own weight and the friction coefficient is measured.

Two steps have been defined to carry out the numerical analyses. Firstly, bolt pretension or clamping force due to bolt tightening is applied using the bolt load command in ABAQUS. The tightening torque creates compression at the holes vicinity of the plates and tension in the bolt shank. In order to apply a bolt load using bolt load option, a cross section through the bolt shank and the axis of the bolt shank is defined. In the second step, one end of the model is fixed and longitudinal displacement is applied to the other end.

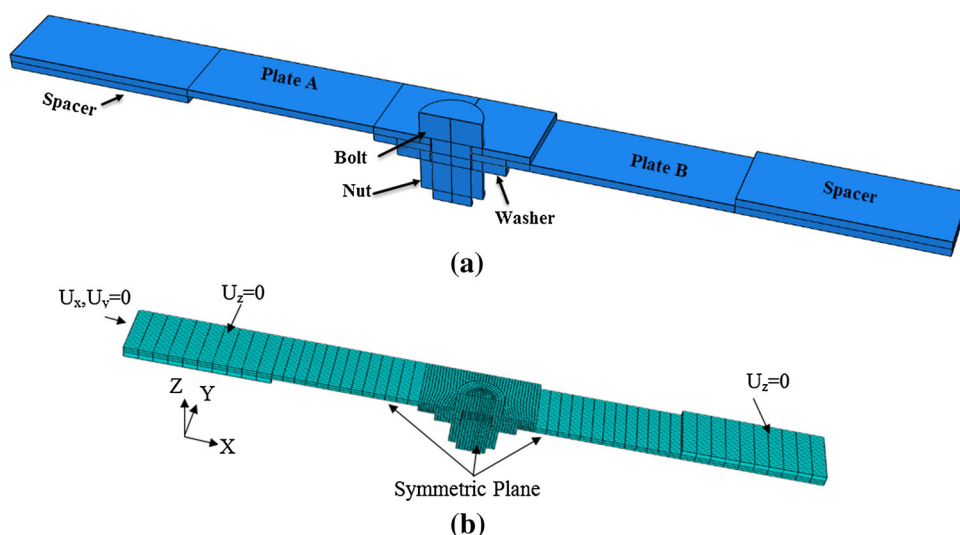
Figure 4a demonstrates the single lap joint components. Also, the FE mesh of the single lap joint specimen is shown in Fig. 4 together with its corresponding boundary conditions. To reduce the computational time, half specimen is modeled due to symmetric condition. Therefore, symmetric boundary condition is applied to the corresponding plane as shown in Fig. 4b. Also, in order to reduce the model complexity, bolt and nut have been assumed to be cylindrical in the FE model.

4 Results and Discussion

This paper studies the distortion and failure behavior of the single lap bolted joints experimentally and numerically. For this purpose three case studies are defined. These cases involve similar and dissimilar material joints. Uni-axial tensile tests have been carried out to study the distortion and failure behavior of the assemblies. Excessive distortions have been observed during the tensile tests. In order to simulate the joint behavior, a nonlinear FE approach has been used.

It is highlighted that practically, both net-section and shear-out failure may be eliminated by designing the joint with adequate edge distance and end distance, respectively.

Fig. 4 Single lap joint model. **a** Joint component, **b** finite element mesh and boundary condition



Therefore in practical design, the bearing failure is checked as the only mode of failure. In this research, the joints have been designed with sufficient edge and end distances to prevent shear-out and net-section failure. The aim of this research is to present a numerical approach which is able to predict the bolted joint distortions, ultimate failure load and the region which is most susceptible for crack initiation in the joints with mixed mode failure.

4.1 Test Results and Model Validation

Plates with similar and dissimilar materials are assembled together with the dimensions as shown in Fig. 3. The uni-axial tensile test has been carried out on a Zwick tensile test machine. The crosshead displacement speed is set at a rate of 1 mm/min. Two spacers have been used to compensate the offset created by the lap joint (see Fig. 4a). Load–displacement diagrams are recorded and used to validate the FE results.

The same geometry and dimensions as the experimental specimens are used to generate the FE models. Static-implicit method is used to simulate the joint behavior. Rate-independent plasticity with Mises yield isotropic hardening rule is used in modeling the response of assemblies. Mises yield criterion states that yielding occurs when the second deviatoric invariant reaches a critical value. This criterion can be written as Eq. 4. Where

$$\phi(\sigma, \alpha) = \bar{\sigma}(\sigma) - Y(\alpha) \tag{4}$$

where $Y(\alpha)$ is the uni-axial yield stress and $\bar{\sigma}$ is the equivalent or Mises stress which can be expressed as Eq. 5. In this equation σ' and σ are deviatoric and Cauchy stress tensors, respectively.

$$\bar{\sigma}(\sigma) = \sqrt{3J_2(\sigma'(\sigma))} \tag{5}$$

The Mises yield function with associated flow means that there is no volumetric plastic strain; since the elastic bulk modulus is quite large, the volume change will be small. Plastic flow rule is defined in terms of plastic multiplier $\dot{\lambda}$ and flow vector $N(\sigma, A)$ as:

$$D^p = \dot{\lambda}N(\sigma, A) \tag{6}$$

Figure 5 illustrates the deformations and failure modes of the plates after loading. As can be seen from Fig. 5, bearing failure occurs in the steel–steel and aluminum–aluminum joints and bearing and cleavage failure is observed in the steel–aluminum joint. From this, it can be inferred that, although the joints with same dimensions are tested, however, for the joints with dissimilar substrates, the failure mode is different.

In order to verify the FE model, diameter of the holes have been measured in the case studies 1 and 2 after loading and have been compared with numerical results. As can be seen from the figure, good agreements are observed

between the results. It is noted that the measurements have been made on the plates which underwent higher distortions and damages (see Fig. 4a for plate A and B). Also maximum principle stress contours are shown in Fig. 5. As can be seen from Fig. 5c, the crack initiates from the point with higher principle stress.

A comparison of load–displacement data obtained from the uni-axial tests and numerical method verifies the FE models. In the FE simulation, displacement is defined as boundary condition and reaction force is requested as history output. Figure 6 compares the total reaction force obtained from the FE model and the load applied in the experiments.

In this research, the Standard Error Estimation (SEE) function (Eq. 7) has been used to calculate the error between the results of the FE simulation and experimental data.

$$SSE = \sqrt{\sum_{i=1}^n \frac{1}{n} (D_{Exp} - D_{FE})_i^2} \tag{7}$$

in which n is the number of data points, D_{Exp} is the deformation measured in each test and D_{FE} is the deformation which is obtained using FE simulation. Error estimation shows that the SEE values for case studies 1–3 are 5, 4 and 26 % respectively. The estimated error in the case study 1 and 2 are negligible, but the reason for high value of the SSE for the case study 3 is attributed to ignorance of damage in the FE simulation. Besides, Fig. 6c shows that the FE method overestimates the ultimate tensile strength of the joint. This reveals the fact that for case study 3, with mix-mode failure, the FE model without considering damage is not accurate.

4.2 Failure Simulation

In this research, uncoupled Cockcroft–Latham ductile fracture criterion, which is the integral damage value, has been employed to predict the failure of the substrates (see Eq. 8). The main advantage of the uncoupled material models is that, they are easy to calibrate and are highly useful for practical applications. In additions, these models can be employed with any hardening functions. Cockcroft–Latham model uses the maximum principle stress, equivalent strain and a material constant C to express the amount of ductile damage. This material constant is critical plastic work per unit volume. Based on Cockcroft–Latham criterion, material fails when the work reaches the critical value.

$$\int_0^{\epsilon_r} \max(\sigma_1, 0) d\epsilon = C \tag{8}$$

In this equation, σ_1 is the maximum principle stress, ϵ_r is the equivalent strain at fracture and C is the critical parameter of damage. The value of the critical parameter of

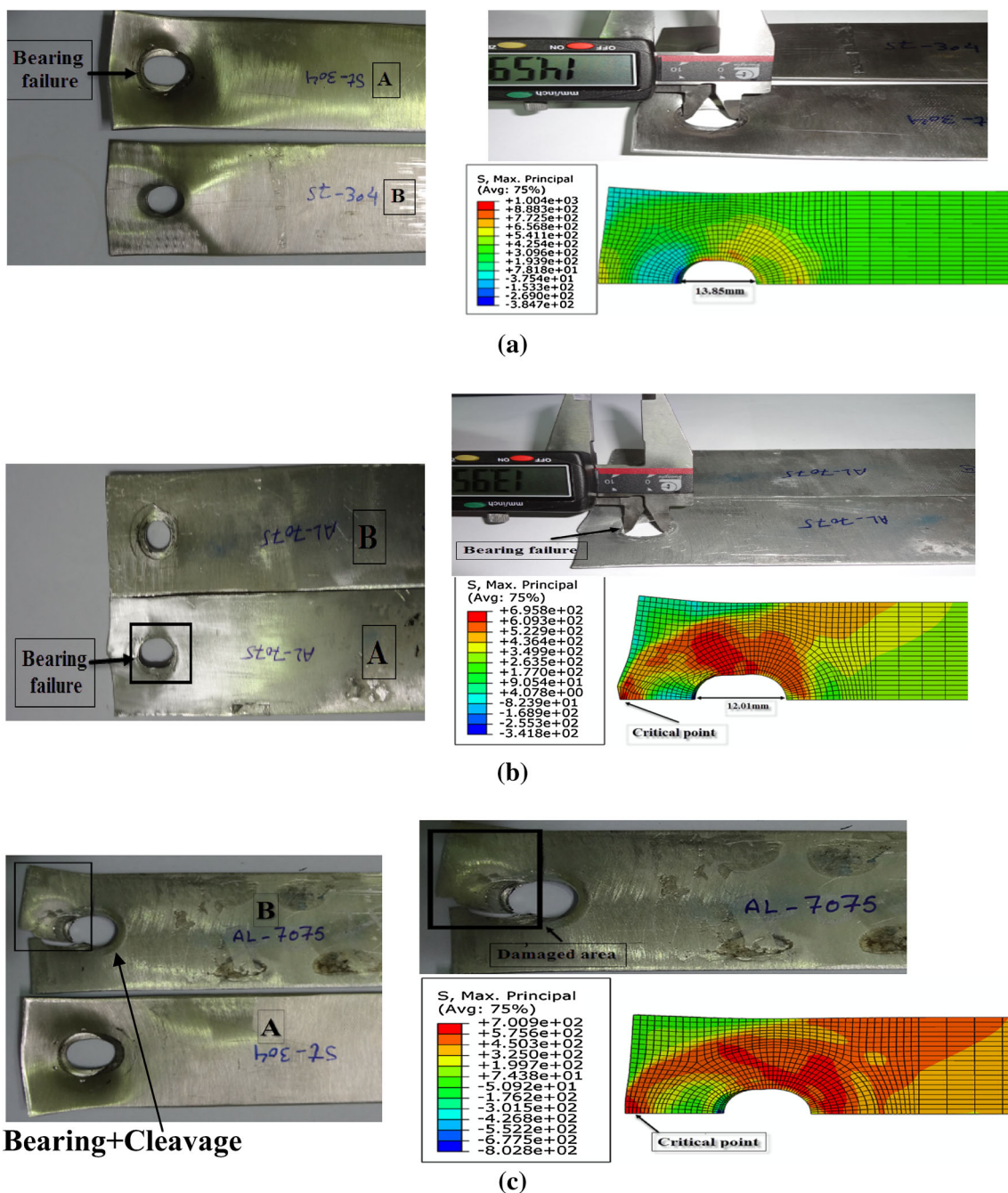


Fig. 5 Deformations and failure modes of the plates after loading. a Case study 1, b case study 2 and c case study 3

damage is assumed constant and is calculated by the integral over stress–strain curve of the material behavior (Fig. 2). Therefore in a tensile test of a smooth specimen, the principle stress σ_1 in Eq. 8 is considered $\sigma_1 = \bar{\sigma}$. Hence the critical value of damage is obtained from Eq. 9. In this equation $\bar{\sigma}$ and $\bar{\epsilon}$ are the equivalent stress and strain, respectively. Table 2 presents the mechanical properties of the substrates which have been extracted from the uni-axial tensile tests.

$$C = W_{cr} = \int_0^{\bar{\epsilon}_p} \bar{\sigma}(\bar{\epsilon}_p, \dot{\bar{\epsilon}}_p) d\bar{\epsilon}_p \tag{9}$$

By implementing this criteria and element degradation technique in the FE code, joint fracture can be simulated. In this method, element degradation starts when the element energy reaches the specified damage initiation criterion. The element is deleted from the mesh once all the

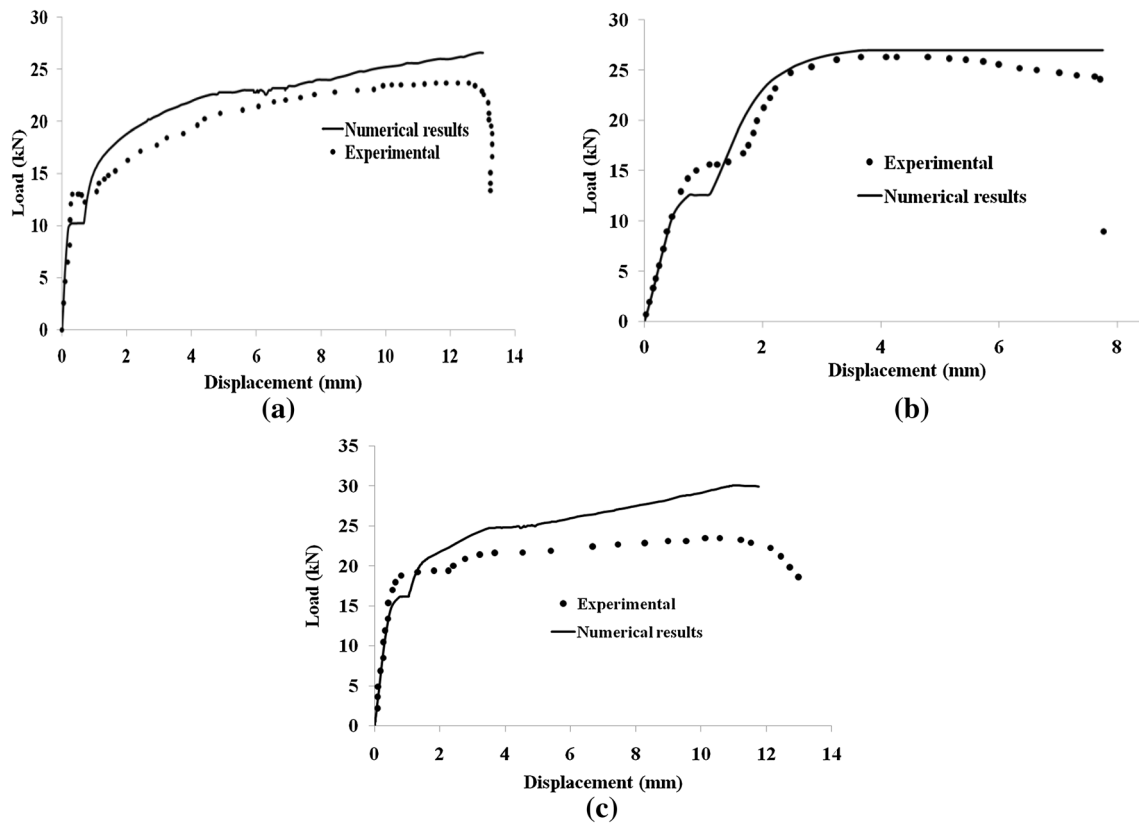


Fig. 6 Comparison between the FE and experimental load–displacement curves. **a** case study 1, **b** case study 2 and **c** case study 3

Table 2 Mechanical properties of substrates

Material	E (GPa)	ν	σ_y (Mpa)	$\sigma_{rupture}$ (MPa)	$\epsilon_{rupture}$ (%)	C (MPa)
St-304	228	0.3	267	1168	62.16	334.5
Al 7075-T6	72	0.3	501	619	13.45	69.3

integration points at any one section of an element fails. It is noted that after the elimination of elements, the total equilibrium of the structure must be ensured. This procedure is introduced to the software using a user defined subroutine.

Figure 7 compares the load–displacement data obtained from FE models with and without damage simulation against test results for case studies 2 and 3. As can be seen from this figure, damage model can accurately predict the lap joint load–displacement curve. Also, this model allows crack initiation simulation; therefore, in this method the joint ultimate strength can be estimated more accurately. In addition, error estimation has been carried out, and the SSE value, for the case 3 is found to be 8 %. It can be concluded from Fig. 7 and SSE values, that more accurate results can be obtained by employing the criteria.

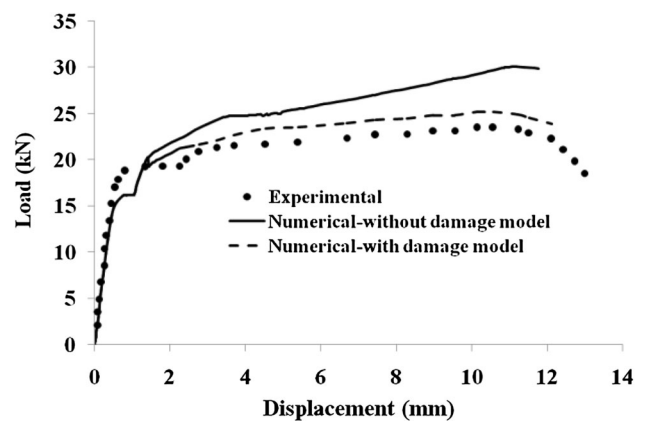


Fig. 7 Comparison between the FE and experimental load–displacement data for case study 3

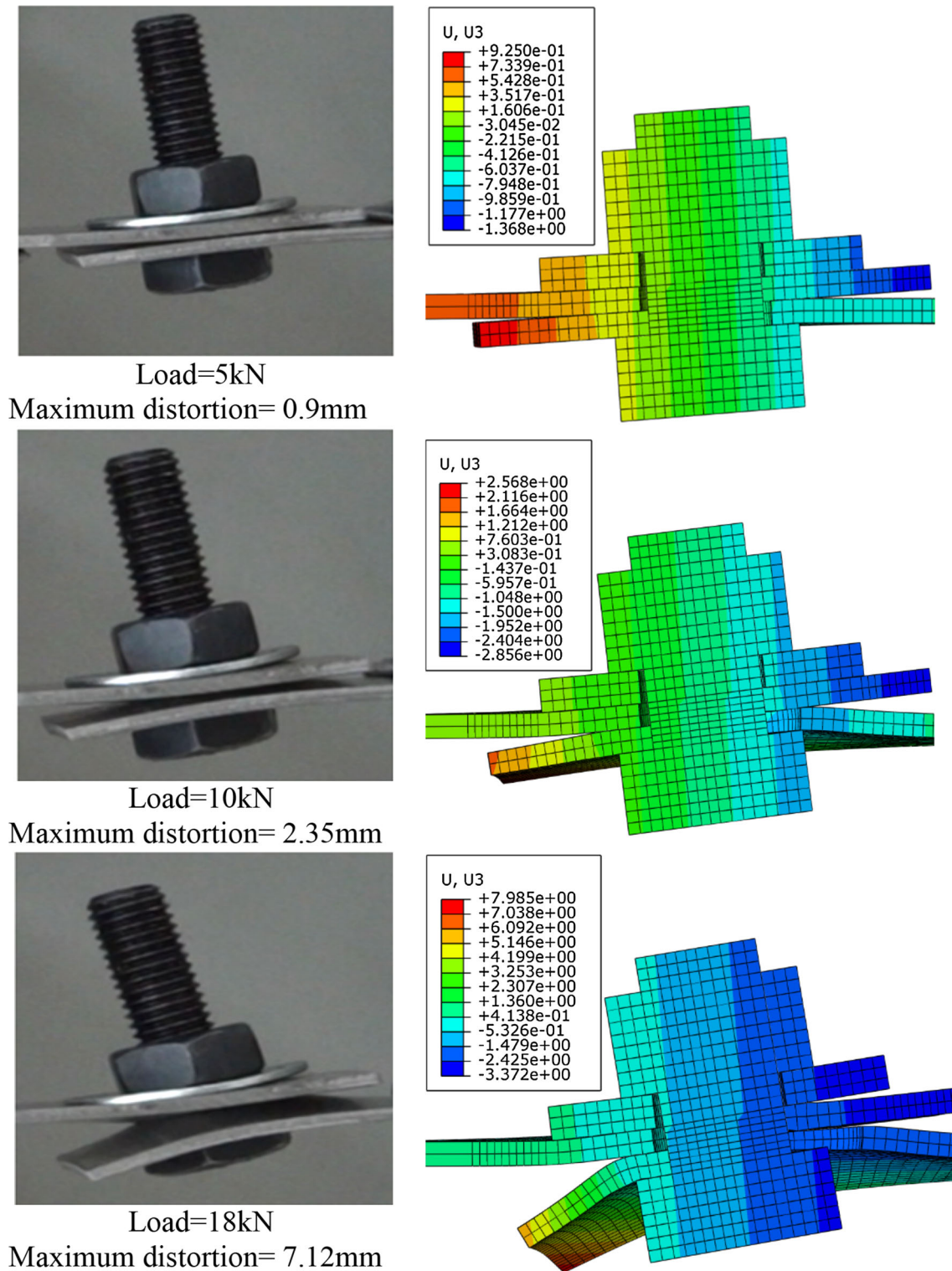


Fig. 8 Comparison between the FE and experimental deformations of the joint in three different loads

Next, the results of the FE simulation with damage model are presented for the case study 3. As can be seen from Fig. 5 the joint with dissimilar materials demonstrate high distortion and damages. In order to capture distortions

and to identify the crack initiation point during the tensile test, four interrupted tests have been carried out. Figure 8 illustrates the deformations of the joint in three different loads before crack initiation. Maximum distortion of the

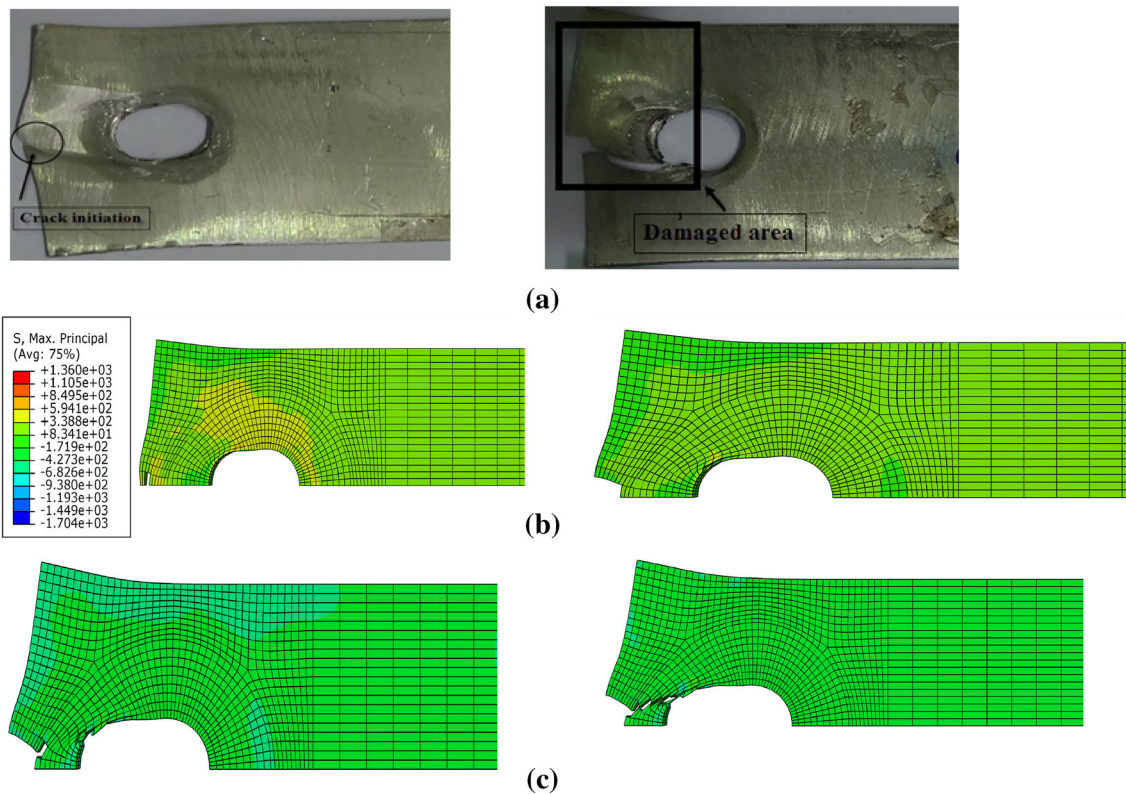


Fig. 9 Aluminum plate failure. **a** Location of damage initiation and final damaged area in the aluminum plate, **b** FE modeling of the damage initiation and rupture of the joint, **c** FE model of the damage growth and complete failure of the plate

joint is measured and compared with the corresponding result obtained from FE model.

Figure 9a shows the location of crack initiation and final damaged area in the Aluminum plate. Crack initiation and rupture are simulated using energy failure criteria and element elimination technique. Figure 9b shows the FE modeling of the crack initiation and rupture of the joint. As can be seen from this figure, FE model predicts the location of the damage initiation accurately. Figure 9c shows that the damage proceeded toward the joint complete failure. Comparing the results of this figure with the damaged area obtained from experiments (see Fig. 9a) shows that Cockcroft–Latham criterion correctly simulated the damaged area. Although in this method, stress singularity in front of crack is ignored and therefore crack propagation cannot be simulated accurately. However the results of this paper shows that, employing the failure model and element degradation, the FE model accuracy can be efficiently increased in predicting the joint distortions and ultimate load.

5 Conclusions

This paper presented the results of the experimental and numerical investigation of the distortion and failure behavior of the single lap bolted joints. Three case studies

were defined to study the distortion and failure behavior of the assemblies. Excessive distortions were observed during the uni-axial tensile tests. Therefore, a nonlinear FE model was used to simulate the joints behavior. Experimental results showed that bearing failure occurred in the steel–steel and aluminum–aluminum joints and mixed mode (Bearing + Cleavage) failure occurred in the aluminum–steel joint. It could be inferred that, although the joints with same dimensions were tested, however for the joints with dissimilar substrates, the failure mode was different.

In addition, FE results showed that elasto-plastic model had sufficient accuracy in predicting the distortion behavior of the models with only bearing failure mode. However, this model had less accuracy compared to the models with Mixed-Mode failure. Results showed that, using a decoupled model based on energy, accurate distortions and ultimate tensile loads of the joints could be obtained in the models with mixed mode failure.

Appendix

User defined subroutine to simulate Cockcroft–Latham failure criterion is appended below.

```

SUBROUTINE USDFLD(FIELD,STATEV,PNEWDT,DIRECT,T,CELENT,
1 TIME,DTIME,CMNAME,ORNAME,NFIELD,NSTATV,NOEL,NPT,LAYER,
2 KSPT,KSTEP,KINC,NDI,NSHR,COORD,JMAC,JMATYP,MATLAYO,
3 LACCFLA)
INCLUDE 'ABA_PARAM.INC'
CHARACTER*80 CMNAME,ORNAME
CHARACTER*3 FLGRAY(15)
DIMENSION FIELD(NFIELD),STATEV(NSTATV),DIRECT(3,3),
1 T(3,3),TIME(2)
DIMENSION ARRAY(15),JARRAY(15),JMAC(*),JMATYP(*),
1 COORD(*)
C Value of current principal stress:
CALL GETVRM('SP',ARRAY,JARRAY,FLGRAY,JRCD,JMAC,JMATYP,
1 MATLAYO,LACCFLA)
PRINC=ARRAY(3)
C Value of updated principal stress:
CALL GETVRM('SDV',ARRAY,JARRAY,FLGRAY,JRCD,JMAC,JMATYP,
1 MATLAYO,LACCFLA)
PRI=ARRAY(3)
C Value of current equivalent strain:
CALL GETVRM('PE',ARRAY,JARRAY,FLGRAY,JRCD,JMAC,JMATYP,
1 MATLAYO,LACCFLA)
PEEQ=ARRAY(7)
C Value of updated equivalent strain:
CALL GETVRM('SDV',ARRAY,JARRAY,FLGRAY,JRCD,JMAC,JMATYP,
1 MATLAYO,LACCFLA)
PQ=ARRAY(2)
C Value of updated damage parameter:
CALL GETVRM('SDV',ARRAY,JARRAY,FLGRAY,JRCD,JMAC,JMATYP,
1 MATLAYO,LACCFLA)
TOTDAM=ARRAY(5)
IF(PRINC.NE.0.0D0)THEN
  IF(TOTDAM.LE.334)THEN
    PLASINC=PEEQ-PQ
C Computing Damage factor by trapezoidal integration:
MNST=(PRINC+PRI)/2
DAMAGE=MNST*PLASINC
C Store the damage parameter as a solution dependent state
C variable
STATEV(1)=DAMAGE
C Update solution dependent state variables:
STATEV(2)=PEEQ
STATEV(3)=PRINC
STATEV(4)=PQ
IF(DAMAGE.GT.0)THEN
  TOTDAMSO FAR=TOTDAM+DAMAGE
  STATEV(5)=TOTDAMSO FAR
ELSE TOTDAMSO FAR=TOTDAM
  STATEV(5)=TOTDAMSO FAR
END IF
END IF
END IF
FIELD(1)=0.D0
IF(TOTDAM.GT.334)THEN
  FIELD(1)=1D0
END IF
C If error, write comment to .DAT file:
IF(JRCD.NE.0)THEN
  WRITE(6,*) 'REQUEST ERROR IN USDFLD FOR ELEMENT NUMBER ',
1 NOEL,'INTEGRATION POINT NUMBER ',NPT
ENDIF
RETURN
END

```

References

1. Theocaris, P S and Demakos C, *Eng Fract Mech* **43** (1992) 501.
2. Thoppul S D, Finegan J, and Gibson R F, *Compos Sci Technol* **69** (2009) 301.
3. Chung K, and Ip K, *Eng Struct* **22** (2000) 1271.
4. Bayton D A F, Long R, and Fourlaris G, *Mater Des* **30** (2009) 635.
5. Korin I, and Ipiña J P, *Int J Fatigue* **33** (2011) 166.
6. Dang Hoang T, Herbelot C, and Imad A, *Eng Struct* **32** (2010) 2793.
7. Aceti R, Ballio G, Capsoni A, and Corradi L, *J Constr Steel Res* **60** (2004) 1333.
8. Dang Hoang T, Herbelot C, Imad A, and Benseddiq N, *Finite Elem Anal Des* **67** (2013) 56.
9. Sen F, Pakdil M, Sayman O, and Benli S, *Mater Des* **29** (2008) 1159.
10. Dang Hoang T, Herbelot C, and Imad A, *Eng Fail Anal* **24** (2012) 9.
11. Salih E L, Gardner L, and Nethercot D A, *J Constr Steel Res* **66** (2010) 1455.
12. Yun J-H, Choi J-H, and Kweon J-H, *Compos Struct* **108** (2014) 409.
13. Shigley J E, *Shigley's Mechanical Engineering Design*, Tata McGraw-Hill Education, New Delhi (2011).